

Activation energy in the thermal decomposition of MgH₂ powders by coupled TG–MS measurements

Part II. Catalytic effects of tin oxide doping

Renzo Camprostrini · Mahmoud Abdellatif ·
Matteo Leoni · Paolo Scardi

Received: 12 June 2013 / Accepted: 19 November 2013 / Published online: 11 December 2013
© Akadémiai Kiadó, Budapest, Hungary 2013

Abstract The catalytic effect of SnO₂ doping on the hydrogen thermal desorption of MgH₂ was investigated by coupled thermogravimetric–mass spectrometric (TG–MS) analyses, among a set of samples prepared with different SnO₂/MgH₂ molar ratios. A small release of water and carbon dioxide was detected at temperatures preceding to the reductive thermal decomposition of MgH₂ yielding molecular hydrogen. While TG and DTA data collected at different heating rate provided an apparent activation energy for the entire thermal process, appropriate ion-current signals from the MS-data were used to obtain the activation energies of the single chemical reactions yielding the formation of H₂O, CO₂, and H₂. The most common equations derived from model-free isoconversion methods (Kissinger–Akahira–Sunose; Flynn–Wall–Ozawa; Starink) were used by processing temperatures referred to the different kinds of signals (TG-, DTG-, DTA-, TIC-, molecular-ion IC-curves) for isoconversion points corresponding to the maximum rate of transformation. Temperature and activation energy values were used to compare the kinetic behavior of MgH₂ powder with the best performance of a doped sample, prepared by high energy grinding of SnO₂/MgH₂ mixture. Doped-MgH₂ samples prepared with SnO₂ mass ratio of 0.2 showed the best kinetic thermal

decomposition behavior, with respect to the pristine MgH₂ powder: a decreasing of the main thermal decomposition event of ca. 51–57 °C associated to a coherent decreasing of ca. 20 % (ca. 30 kJ mol⁻¹) of its activation energy value.

Keywords Activation energy · Magnesium hydride decomposition · Mass-spectroscopic analyses · Hydrogen release thermal analysis · Ball milling · Nanocrystalline materials · Catalytic effect of SnO₂

Introduction

Thermodynamics and kinetics currently limit the practical application of magnesium hydride for hydrogen storage [1, 2]. The enthalpy of formation ($\Delta H^{\text{of}} = -76 \text{ kJ mol}^{-1}$) is in fact too high for a competitive application, e.g., in proton exchange membrane fuel cells.

Recent studies point out that hydrogen evolution during heating of MgH₂ powders proceeds in two stages:

- (i) rapid nucleation and growth of metallic magnesium inside hydride particles, occurring when temperature exceeds a certain critical threshold;
- (ii) associative hydrogen desorption from the surface of the solid solution of H in Mg.

The latter is the rate-limiting step [3].

Mechanical milling or co-milling with a nanosized catalyst is the most common method to overcome the above cited disadvantages [4, 5]. In fact, the reactive impacts occurring during high-energy ball milling yield both the reduction of particle size and the introduction of structural defects that can act as additional paths for hydrogen transport, thus providing kinetic and thermodynamic

R. Camprostrini
DII, University of Trento, via Mesiano 77, 38123 Trento, Italy

M. Abdellatif · M. Leoni (✉) · P. Scardi
DICAM, University of Trento, via Mesiano 77, 38123 Trento, Italy
e-mail: matteo.leoni@unitn.it

M. Abdellatif
Elettra Sincrotrone, S. S. 14 - km 163.5, 34149 Basovizza, Trieste, Italy

benefits. Moreover, ball milling usually leads to the transformation of the equilibrium β -MgH₂ polymorph into the metastable γ -MgH₂ (high pressure polymorph).

Although with no data support, the supposedly lower enthalpy of formation is claimed to justify the lower hydrogen desorption temperature exhibited by γ -MgH₂ with respect to β -MgH₂ in milled MgH₂ powders [4]. Transition metals [6–12], oxides [13–16], and halides [17] are typical catalysts employed to dope MgH₂ with the intent of lowering both the temperature of decomposition to molecular hydrogen and the energy demand of the related process. Unfortunately, the beneficial effects on MgH₂ are mostly limited to the kinetic properties (e.g., hydrogen absorption/desorption rate), whereas the (unfavorable) thermodynamics parameters are largely unaffected.

As presented in the first part of this work [18], the basic kinetic and thermodynamic parameters of a MgH₂ sample ($H_{2(g)}$ -release temperature and activation energy) can be easily obtained from coupled TG and MS measurements. TG–MS data—in particular the evolved gas phase analysis, EGA—provide a detailed picture of the thermal transformations occurring in the solid sample. Moreover, further information can be obtained on the real chemical nature (composition) of the initial powder specimen.

In this paper, the thermal decomposition of a set of SnO₂/MgH₂ samples produced with increasing molar ratios was studied by coupled TG–MS and by X-ray diffraction, and compared with the intrinsic behavior of an unmilled- and undoped-MgH₂ specimen. The catalytic effects of SnO₂ on the $H_{2(g)}$ desorption process were also investigated through TG–MS experiments carried out at different constant heating rates in order to determine apparent activation energies of the whole process and of its reactions pattern [19, 20].

Experimental

Chemical products

Commercial magnesium hydride (MgH₂, 96.5 % purity) and tin(IV) oxide (SnO₂, 99.9 % purity) powders were purchased from Sigma-Aldrich and used as-received. Two stocks of MgH₂ powder (of the same trademark and quality) were used. Reagents and samples were kept and handled under argon atmosphere (99.999 % purity) inside a glove-box.

Sample preparation

A set of SnO₂/MgH₂ samples was prepared by mechanical mixing of the MgH₂ and SnO₂ powders. Specimens with

nominal SnO₂/MgH₂ mass ratio of 0.05, 0.10, 0.15, and 0.20 were produced, labeled in the following as SnO₂/MgH₂ = *N*, where *N* represents the mass ratio value. The whole procedure was conducted in the glove-box under Ar atmosphere. Appropriate amounts of the two pure compounds were ground in a Pulverisette 4 (Fritsch, Germany) planetary mill with a hardened Cr-steel milling set (volume of the jar 80 cm³) loading the sample into the jar inside the glove-box, adding 10 Cr-steel balls (diameter 12 mm) to get a powder/ball mass ratio = 1/47. The powders were milled for 16 h with a speed of 200 rpm and a gear ratio $\Omega/\omega = -1$. The sample of composition SnO₂/MgH₂ = 0.2 was then selected and its thermal behavior compared with that of the MgH₂ commercial powders previously analyzed.

Instrumentations

Thermogravimetry (TG) and differential thermal analyses (DTA) were performed on a Setaram LabSys thermobalance, operating in the range of 20–600 °C under a constant He flow (120 cm³ min⁻¹). Similar amounts of the various SnO₂/MgH₂ mixtures (13–16 mg) were analyzed by using α -Al₂O₃ (8.7 mg) as a reference. For the kinetic study, TG–MS measurements were carried out at different linear heating rate $\beta = 7, 10, 13, 16, 19, 22, \text{ and } 25$ °C min⁻¹. Further details on the operative conditions and on the set up of the transfer line, used to connect the TRIO-1 VG quadrupole mass spectrometer detector with the thermobalance furnace, are reported in Part 1 [18]. Mass spectra (electron impact 70 eV) were recorded in the range of 1–400 amu with frequency of 1 scan s⁻¹.

From the recorded MS data, the total ion-current curve (TIC graph) and the contribution of selected *m/z* ion currents (IC graphs) can be plotted versus time to pair the linear temperature increase of the coupled thermal analysis. The TIC curve monitors the total gas phase release, whereas appropriate *m/z* IC curves can monitor the evolution of one species independently from the presence of others. Moreover, the area of the bands detected in the IC curves allows a semiquantitative evaluation of the relative amounts of the evolved species. These values can be compared among different TG–MS measurements if a normalization is done with respect to the amount of analyzed sample and to the (constant) inert He flow (i.e., the integrated area of the *m/z* = 4 ion-current signal) [21–24].

X-ray diffraction data were collected on a Rigaku PMG/VH diffractometer equipped with a CuK_α tube source (40 kV and 30 mA) and a graphite crystal monochromator on the diffracted arm. Instrument optics (1° divergence and antiscatter slits, 2° primary and secondary Soller slits) guarantee a narrow and symmetric profile throughout the employed 20°–80° 2θ range; data were collected in

0.05° step mode with 5 s counting time. The PANalytical HighScore 2.2 software was used for phase identification, whereas Bruker TOPAS v.4.2 based on the Rietveld method was employed for the quantitative data analysis [25].

Results

The intrinsic thermal behavior of the as-received (i.e., unmilled) MgH₂ sample, described in the first part of this work [18], is here briefly summarized (referring to TG–MS analysis at $\beta = 10 \text{ }^\circ\text{C min}^{-1}$):

- (A) a first small broad mass loss event (40–390 °C, 1.6 mass% intensity), which is correlated with two global gas phase evolutions of water and carbon dioxide as detected by the TIC curve (peak at 86 and 312 °C);
- (A.1) in this temperature range H₂O is released in two distinct events (at 89 and 315 °C), while CO₂ evolution is detected in a main event (at 325 °C) preceded by two small broad and overlapped releases (at 100 and 244 °C), as detected by the respective IC $m/z = 18$ and 44 curves;
- (B) the main mass loss (at 433 °C, 7.0 mass%), leading to strong sharp TIC peak at 440 °C;
- (B.1) this release corresponds to the molecular hydrogen evolution (at 440 °C) with traces of water (at 439 °C) as indicated by the respective IC $m/z = 2$ and 18 curves.

The thermal behavior of the milled MgH₂ powders (TG–MS at $\beta = 10 \text{ }^\circ\text{C min}^{-1}$ on 11.2 mg of the second stock) shows a TG curve with a unique mass loss of 5.8 mass%; both DTG and DTA curves indicate a sharp band at 379 °C (not shown for brevity). EGA presents a TIC curve

characterized by a unique peak centred at 385 °C. H₂ release is described by a symmetric peak at 388 °C in the $m/z = 2$ IC curve. H₂O evolution ($m/z = 18$ IC) gives rise to a modest band at 90 °C with a prolonged tail effect overlapped with a weak band at 290 °C and followed by a second more intense band at 384 °C. CO₂ release ($m/z = 44$ IC) starts at ca. 250 °C, showing a scarcely detectable band at 382 °C.

A preliminary set of TG–MS measurements (all carried out at $\beta = 10 \text{ }^\circ\text{C min}^{-1}$) was employed to compare the catalytic performance of the various SnO₂-doped MgH₂ samples and to select the best candidate specimen for the subsequent kinetic study. The thermal decomposition of the MgH₂ component was analyzed taking into account different parameters: the onset and peak temperature of the DTA-band curve; the peak temperature of the DTG-band curve; the mass loss of the TG-curve during the H-release event. Analogously, the onset, peak temperature and peak area of the $m/z = 2$ ion-current were considered from the MS data. The most representative results of this screening are summarized in Table 1.

The values of the TG mass loss and the integral of the DTG and $m/z = 2$ IC bands were also normalized considering either the nominal SnO₂/MgH₂ composition or the combined mass percentage of the β - and γ -MgH₂ phases, as experimentally determined by the XRD analyses. X-ray results (object of a separate work [26]) detected the presence of four phases in the SnO₂/MgH₂ samples, whose mass percentages are reported in Table 2. The unmilled MgH₂ sample is mostly composed of tetragonal β -MgH₂ phase. Milling induces a transformation of the material, with a substantial quantity of γ -MgH₂ forming together with nanostructured MgO. In all SnO₂-doped MgH₂ samples the γ -MgH₂ polymorph is present in low and almost constant amount, whereas the fraction of MgO is higher

Table 1 Some characterization data of pure MgH₂ samples and of the set of SnO₂/MgH₂ specimens of different composition, from TG–MS analyses ($\beta = 10 \text{ }^\circ\text{C min}^{-1}$). *r.u.* relative units

| Sample label | Thermal analyses | | | | MS analysis | | | |
|-------------------------------------------|-----------------------------------|----------------------------------|----------------------------------|-----------------------------|-----------------------------------|----------------------------------|------------------------|------------------------|
| | DTA band | | DTG band | TG curve | IC $m/z = 2$ band | | | |
| | $T_{\text{onset}}/^\circ\text{C}$ | $T_{\text{peak}}/^\circ\text{C}$ | $T_{\text{peak}}/^\circ\text{C}$ | Mass loss/mass ^a | $T_{\text{onset}}/^\circ\text{C}$ | $T_{\text{peak}}/^\circ\text{C}$ | Area/r.u. ^b | Area/r.u. ^c |
| Pure unmilled MgH ₂ | 413 | 444 | 444 | 7.6 | 418 | 450 | 7.1 | 7.1 |
| Pure milled MgH ₂ | 360 | 379 | 379 | 6.2 | 354 | 388 | 4.1 | 4.3 |
| SnO ₂ /MgH ₂ = 0.05 | 349 | 384 | 385 | 6.7 | 340 | 390 | 3.8 | 4.4 |
| SnO ₂ /MgH ₂ = 0.10 | 352 | 377 | 377 | 6.6 | 328 | 383 | 5.0 | 6.0 |
| SnO ₂ /MgH ₂ = 0.15 | 348 | 386 | 380 | 7.3 | 311 | 392 | 4.7 | 6.0 |
| SnO ₂ /MgH ₂ = 0.20 | 348 | 378 | 376 | 7.5 | 296 | 388 | 5.5 | 6.8 |

^a Calculated with respect to the mass% of β - and γ -MgH₂ phases detected by XRD analysis in each sample (theoretical value 7.659 mass%)

^b Normalized with respect to He Flow of the TG–MS measurements and to the nominal mass% of MgH₂ used in the sample preparation

^c Normalized with respect to He Flow of the TG–MS measurements and to the mass% of β - and γ -MgH₂ phases detected by XRD analysis in each sample

and slightly increases with the SnO₂ content. The estimated amount of SnO₂ is close to the nominal composition of the powder mixture.

The SnO₂/MgH₂ = 0.2 sample, providing the best tradeoff between reduction of the H₂-release temperature and reduction of the hydrogen storage capacity, was selected for the subsequent kinetic study. To quantify the amount of H₂ released, the TG mass loss and the area of the $m/z = 2$ IC band were considered. The trend of these parameters is shown in Fig. 1.

The thermal behavior of the SnO₂/MgH₂ = 0.2 sample is described by the TG–MS analysis carried out on 14.3 mg at $\beta = 10 \text{ }^\circ\text{C min}^{-1}$, as shown in Fig. 2. The TG curve shows a modest linear mass loss in the range 40–300 °C (0.5 % intensity), followed by a net event of 5.3 % in the range 300–425 °C. The DTA curve shows a narrow and symmetric endothermic peak at 378 °C, while DTG presents a broader and front-asymmetric peak centered at 376 °C. The TIC curve shows a modest and broad band at 96 °C, and a more intense one centered at 383 °C, with a small shoulder at ca. 340 °C. The release of molecular hydrogen from this doped sample is described by a sharp peak at 384 °C, preceded by a quite modest plateau in the range 300–350 °C, as shown by the $m/z = 2$ IC signal. The $m/z = 18$ IC curve (water release), shows a main band at 102 °C, a very small plateau in the interval 200–240 °C and a modest band at 384 °C. Carbon dioxide evolution ($m/z = 44$ IC) is detected in three events: a most intense band at 102 °C, a smaller one at 381 °C and a less intense and broad one at 253 °C.

The thermal behavior of the pure SnO₂ powder sample was also examined by TG–MS, carried out at $10 \text{ }^\circ\text{C min}^{-1}$ (up to 500 °C) on 8.5 mg of specimen (not shown for brevity). The TG curve indicates a negligible mass loss up to ca. 180 °C, whereas the TIC curve presents a scarcely detectable but very broad band in the 50–150 °C range. The water ($m/z = 18$) IC curve reveals a first small band centered at 100 °C and a second even smaller and broader one at 390 °C. Carbon dioxide ($m/z = 44$ IC) also shows a very small and broad band around 400 °C (similar to the water evolution), although the release of CO₂ only regards

trivial amounts, as can be deduced from the comparison between the integrated areas under these two IC bands.

Similarly to the behavior of the pristine (unmilled) MgH₂ sample (see Part 1 [18]), the thermal trend of the SnO₂/MgH₂ = 0.2 sample is not related to the heating rate of the various TG–MS measurements (β values in the 7–25 °C min⁻¹ range), although some differences are evidenced with respect to the pristine MgH₂ specimen.

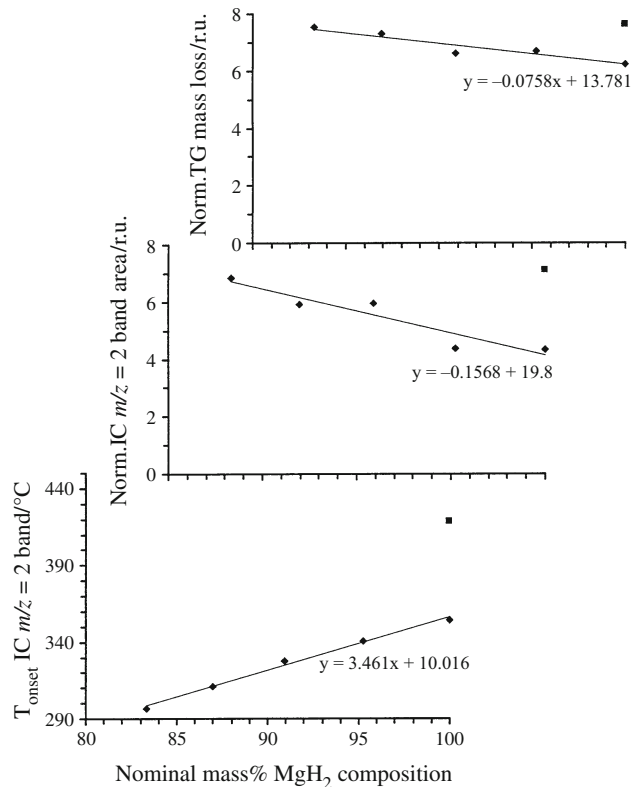


Fig. 1 Trend of the main parameters used to monitor and to quantify the hydrogen release in the TG–MS analyses ($\beta = 10 \text{ }^\circ\text{C min}^{-1}$): of the pure unmilled (pristine) MgH₂ sample (filled square); of the pure milled MgH₂ sample (filled diamond); of the set of the SnO₂-doped samples of different SnO₂/MgH₂ composition (filled diamond). IC $m/z = 2$ band area and TG mass loss values were normalized by the β - and γ -MgH₂ phases content, as detected in the XRD analyses. *r.u.* relative units

Table 2 Some characterization data of pure milled MgH₂ sample and of the set of SnO₂/MgH₂ specimens of different composition, from XRD analyses

| Sample label | Nominal composition | | Composition from XRD analyses | | | |
|-------------------------------------------|-------------------------|-------------------------|----------------------------------|-----------------------------------|-----------|-------------------------|
| | SnO ₂ /mass% | MgH ₂ /mass% | β -MgH ₂ /mass% | γ -MgH ₂ /mass% | MgO/mass% | SnO ₂ /mass% |
| Pure milled MgH ₂ | 0 | 100 | 79.9 | 14.1 | 6.0 | 0 |
| SnO ₂ /MgH ₂ = 0.05 | 4.8 | 95.2 | 77.9 | 4.2 | 13.4 | 4.5 |
| SnO ₂ /MgH ₂ = 0.10 | 9.1 | 90.9 | 71.3 | 4.8 | 14.2 | 9.7 |
| SnO ₂ /MgH ₂ = 0.15 | 13.0 | 87.0 | 65.3 | 4.2 | 16.8 | 13.7 |
| SnO ₂ /MgH ₂ = 0.20 | 16.7 | 83.3 | 62.8 | 4.2 | 16.2 | 16.8 |

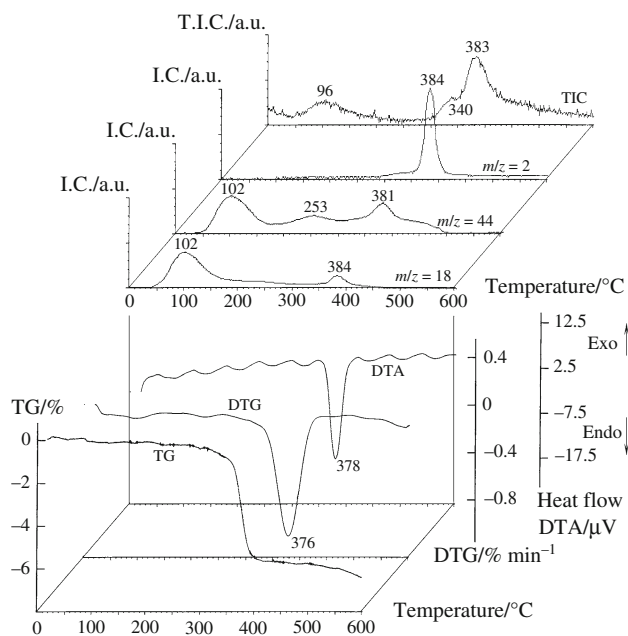


Fig. 2 TG–MS analysis of SnO₂/MgH₂ = 0.2 sample carried out at 10 °C min⁻¹ heating rate

Table 3 reports the increase of the temperatures of all events recorded for the selected signals in the various TG–MS measurements.

Discussion

The main detected event in the thermal behavior of all the SnO₂-doped (ball milled) samples was the evolution of molecular hydrogen due to the reductive decomposition of

MgH₂ to magnesium. The event always occurred at temperatures lower than in the unmilled MgH₂ sample, up to 65–70 °C less in the case of the best performer (SnO₂/MgH₂ = 0.2). Moreover, based on the corresponding TG–MS analysis, no particular contributions of SnO₂ can be evidenced in the thermal behavior of the SnO₂/MgH₂ samples, apart from a small increase in the amount of released water. However, it must be reminded that doped samples have been prepared with a completely new package of MgH₂, which was more rigorously kept and handled under an inert atmosphere.

Taking this last aspect into account, we can compare the small differences detected in the MS data between the pristine and the milled MgH₂ samples. If the different trends of the (small amounts of) released water and carbon dioxide can be neglected, the relevant temperature decrease in the H₂-release constitutes the important effect of the milling process. Actually, milling advantage is limited to the downward temperature being associated with an unfavorable reduced H₂-storage capability, as revealed by the lower released H₂ amount found for the ground sample.

The downward H₂-release temperature shift of SnO₂/MgH₂ samples depends both on the catalytic effect of SnO₂, but also on the operative milling conditions [2]. Although all these aspects play a fundamental role in preparing materials ultimately devoted to practical applications, in this second work our main attention is still focused on the comparison of the activation energies of all the thermal-decomposition events of the material as determined by the simultaneous processing of thermal and mass spectrometric data.

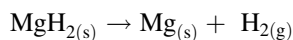
The thermal behavior of the SnO₂/MgH₂ = 0.2 sample is similar to that of the undoped MgH₂ powder, with the

Table 3 TG–MS analyses of SnO₂/MgH₂ = 0.2 milled-sample

| Heating rate of TG–MS analysis, β/°C min ⁻¹ | 7 | 10 | 13 | 16 | 19 | 22 | 25 |
|--------------------------------------------------------|-------|-------|-------|-------|-------|-------|-------|
| Data from TG–DTA analyses | | | | | | | |
| TG-curve T _{flex} | 370.1 | 376.8 | 383.6 | 388.5 | 391.1 | 394.2 | 398.5 |
| DTG-curve T _{peak} | 368.7 | 376.1 | 382.4 | 385.6 | 391.0 | 392.3 | 397.0 |
| DTA-curve T _{onset} | 350.2 | 359.0 | 363.0 | 367.5 | 371.4 | 374.1 | 376.8 |
| DTA-curve T _{peak} | 371.2 | 377.5 | 384.6 | 387.8 | 393.5 | 395.7 | 399.7 |
| Data from MS analysis | | | | | | | |
| TIC-curve 1st band T _{peak} | 82.6 | 96.0 | 106.6 | 115.2 | 123.5 | 132.0 | 138.8 |
| TIC-curve 2nd band T _{peak} | 373.8 | 383.4 | 392.6 | 400.3 | 406.0 | 409.2 | 415.0 |
| IC-curve for m/z = 2, T _{peak} | 375.2 | 384.0 | 393.1 | 397.9 | 405.7 | 409.2 | 415.3 |
| IC-curve for m/z = 18 1st band T _{peak} | 91.7 | 102.0 | 111.2 | 118.6 | 123.3 | 129.8 | 135.3 |
| IC-curve for m/z = 18 2nd band T _{peak} | 374.5 | 383.6 | 392.1 | 397.0 | 403.2 | 408.5 | 412.3 |
| IC-curve for m/z = 44 1st band T _{peak} | 91.6 | 102.3 | 108.8 | 115.5 | 122.4 | 127.6 | 132.8 |
| IC-curve for m/z = 44 2nd band T _{peak} | 245.0 | 252.8 | 260.4 | 265.3 | 269.4 | 273.5 | 277.5 |
| IC-curve for m/z = 44 3rd band T _{peak} | 371.1 | 380.9 | 387.8 | 394.2 | 400.1 | 404.6 | 408.5 |

Temperatures (°C) of constant conversion degree (α) recorded in the various experiments at different heating rates (β)

extra feature of a lower temperature of hydrogen release, caused by the combined catalytic action of milling and SnO₂ addition. In the TG–MS analysis, carried out at $\beta = 10 \text{ }^\circ\text{C min}^{-1}$, the main thermal event occurs at 377–378 °C as detected by the T_{flex} in the TG curve and by the T_{peak} in the DTA band (see Fig. 2). If the presence of the very small amounts of H₂O and CO₂ are neglected, this thermogravimetric event is described by the reaction:



as shown in the mass spectra recorded in correspondence with the development of the TIC peak centered at 383 °C.

Differently from the DTG signal, the TIC curve indicates two thermal events (Fig. 2): a first modest contribution in the 80–140 °C interval, where recorded mass spectra reveal the only presence of water and carbon dioxide, and a second more intense band, characterized by a maximum at 383 °C with a shoulder at ca. 340 °C. This main thermal event is due to the molecular hydrogen release, whose $m/z = 2$ IC presents a single, sharp, and symmetric band centered on 384 °C, preceded by a small plateau in the 300–350 °C interval. This first contribution, at lower temperatures, indicates an incipient thermal decomposition of a small MgH₂ fraction, probably due to the presence of smaller-size crystallites obtained in the mixing and milling process with SnO₂. It is in fact known that milling with the hard SnO₂ phase leads to β -MgH₂ crystallites of smaller dimensions and with an increasing amount of lattice defects, which provide preferential channels for H₂ desorption [4, 12].

Differently from what observed in the pristine MgH₂ (see Part 1 [18]), the water release ($m/z = 18$ IC) shows only two main events (Fig. 2). Actually, the integration of the $m/z = 16 + 17 + 18$ IC curves (used as a parameter to quantify the released moles of H₂O and for a relative comparison with the other chemical species) shows that 73.0 mol% water is released in the 40–300 °C temperature range (i.e., in the first mass loss), and a remaining 27.0 mol% during the second main thermogravimetric event (300–425 °C), which is strictly overlapped with the hydrogen release interval.

The evolution of carbon dioxide is still described by three distinct events, as it was observed for the pristine MgH₂ sample, but these three releases show here a comparable intensity (cf. the $m/z = 44$ IC of Fig. 2). From the integration of the $m/z = 28 + 44$ ion-current curve, 67.6 mol% of CO₂ is released in the 40–300 °C temperature range (i.e., in the first two bands) and the remaining 32.4 mol% in the last thermogravimetric event together with the H₂ formation. From a comparison of the areas below the relative cumulative ion currents, 70.2 and 29.8 mol% are the relative amounts of water and carbon dioxide totally evolved in the whole 40–425 °C interval.

So, taking into account the relative intensity of the two thermogravimetric events (0.5 and 5.3 mass%, respectively), as well as the kind and relative amounts of the evolved species (as deduced by the MS data elaboration), the following thermal decomposition pattern can be deduced:

- (A) during the first mass loss, the released gas is constituted by 71.8 mol % of H₂O and 28.2 mol % of CO₂. These two species yield for the analyzed solid sample a mass loss of 0.26 and 0.25 mass%, respectively;
- (B) during the second mass loss, the gas phase is constituted by 0.2 mol % of H₂O, 0.1 mol % of CO₂, and 99.7 mol % of H₂. The three species contribute to the sample mass loss by 0.09, 0.12, and 5.09 mass%, respectively.

The hydrogen mass loss indicates a real MgH₂ content of 66.4 mass% for the SnO₂/MgH₂ = 0.2 sample; this value is in good agreement with the result found by quantitative XRD analysis (cf. Table 2).

From the TG–MS measurements carried out at increasing heating rates (from 7 to 25 °C min⁻¹), it is also possible to determine the apparent activation energy of the whole thermal process and to better identify the chemical reactions pattern. Recorded data were elaborated by using the four type-B equations corresponding to the methods of Kissinger–Akahira–Sunose, Flynn–Wall–Ozawa and Starink (type-B equations) [27–31]. Details on these models can be found in the cited literature and are also summarized in Part 1 of the present work [18]. Only the iso-conversion points corresponding to the maximum course of the process, or to the maximum evolution of the detected gas-phase species, were considered. This choice is forced by the low intensity of the experimental MS signals and, in turn, by the high uncertainty in determining the correct temperatures when the ion current does not reach the maximum intensity. Tables 4 and 5 report the linear equations and the activation energies calculated according to the four model equations, obtained by extrapolating both TG and MS data previously summarized in Table 3. The $y = E/(RT)$ parameter is also provided as a means to assess the reliability of the isoconversion method employed to quantify the activation energy value [32, 33].

As a general consideration, the activation energies obtained from the TG data seem more consistent for this doped sample than for the undoped MgH₂ sample. By processing the T_{flex} points of the TG curves, activation energies of 152–155 kJ mol⁻¹ were derived, while values of 153–156 kJ mol⁻¹ were obtained from the T_{peak} points of the DTG bands, and values ranging from 153 to 155 kJ mol⁻¹ from the T_{onset} points of the DTA bands (see Table 4). Considering an experimental error of ca. 4 kJ mol⁻¹, all

Table 4 Apparent activation energy values obtained, for SnO₂/MgH₂ = 0.2 sample, from TG–MS coupled measurements by using TG- and MS-data processed with Flynn–Wall–Ozawa (type B-0), Kissinger–Akahira–Sunose (type B-2), and Starink (type B-1.95 and 1.92) equations

| Data from | $T_{\text{isoconversion}}$ point from | Method | Linear equation from interpolated points ^a | R^{2b} | Act. energy/ kJ mol ⁻¹ | y value $y = E/RT$ |
|-----------------|------------------------------------------|--------|----------------------------------------------------------|----------|--------------------------------------|-----------------------|
| TG–DTA analyses | TG-curve T_{flex} | B-0 | $y = -19.585x + 28.311$ | 0.9962 | 155 ± 4 | 28 |
| | | B-2 | $y = -18.271x + 13.335$ | 0.9956 | 152 ± 5 | 28 |
| | | B-1.95 | $y = -18.304x + 13.706$ | 0.9956 | 152 ± 5 | 28 |
| | | B-1.92 | $y = -18.324x + 13.934$ | 0.9956 | 152 ± 5 | 28 |
| | DTG-curve T_{peak} | B-0 | $y = -19.696x + 28.543$ | 0.9944 | 156 ± 5 | 28 |
| | | B-2 | $y = -18.385x + 13.571$ | 0.9935 | 153 ± 6 | 28 |
| | | B-1.95 | $y = -18.417x + 13.945$ | 0.9936 | 153 ± 6 | 28 |
| | | B-1.92 | $y = -18.437x + 14.17$ | 0.9936 | 153 ± 6 | 28 |
| | DTA-curve T_{onset} | B-0 | $y = -19.657x + 29.358$ | 0.9966 | 155 ± 4 | 29 |
| | | B-2 | $y = -18.383x + 14.445$ | 0.9962 | 153 ± 4 | 29 |
| | | B-1.95 | $y = -18.415x + 14.818$ | 0.9962 | 153 ± 4 | 29 |
| | | B-1.92 | $y = -18.434x + 15.042$ | 0.9962 | 153 ± 4 | 29 |
| | DTA-curve T_{peak} | B-0 | $y = -19.205x + 27.689$ | 0.9945 | 152 ± 5 | 28 |
| | | B-2 | $y = -17.888x + 12.709$ | 0.9937 | 149 ± 5 | 27 |
| | | B-1.95 | $y = -17.921x + 13.084$ | 0.9937 | 149 ± 5 | 27 |
| | | B-1.92 | $y = -17.941x + 13.308$ | 0.9937 | 149 ± 5 | 27 |
| MS analysis | TIC-curve 1st band T_{peak} | B-0 | $y = -3.3295x + 7.2277$ | 0.9985 | 26 ± 1 | 8 |
| | | B-2 | $y = -2.564x - 6.6693$ | 0.9969 | 21 ± 1 | 7 |
| | | B-1.95 | $y = -2.5832x - 6.3219$ | 0.9970 | 21 ± 1 | 7 |
| | | B-1.92 | $y = -2.5946x - 6.1134$ | 0.9970 | 22 ± 1 | 7 |
| | TIC-curve 2nd band T_{peak} | B-0 | $y = -13.643x + 18.957$ | 0.9973 | 108 ± 4 | 19 |
| | | B-2 | $y = -12.308x + 3.9511$ | 0.9967 | 102 ± 4 | 18 |
| | | B-1.95 | $y = -12.342x + 4.3262$ | 0.9967 | 103 ± 4 | 18 |
| | | B-1.92 | $y = -12.362x + 4.5513$ | 0.9967 | 103 ± 4 | 18 |

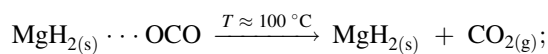
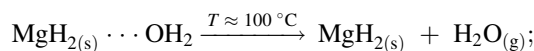
^a From data reported in Table 3^b Correlation coefficient of the linear equation

these numbers represent the same activation energy; whereas, the energies obtained by processing the T_{peak} points of the DTA bands are slightly lower (149–152 kJ mol⁻¹). On the other hand, E values obtained from the T_{peak} points of the first TIC band (centred at 96 °C when $\beta = 10$ °C min⁻¹) are in the 21–26 kJ mol⁻¹ range, and those from the second TIC band (at 383 °C when $\beta = 10$ °C min⁻¹) are of 102–108 kJ mol⁻¹. A direct comparison of those values with literature data is not possible, as the actual values are heavily dependent on the processing conditions (e.g., milling) and morphology of the sample (e.g., powder vs. film). In any case, our values are comparable to literature data for pure MgH₂ (cf. data in [2]).

Activation energies of 30–35 and 32–36 kJ mol⁻¹ were, respectively, derived for the first evolutions of water and carbon dioxide by considering the trend of their respective ($m/z = 18$ and 44) IC (see Table 5). These very close values are consistent with the overlap of the release events for these two compounds, particularly in the TG–MS measurements carried out at the lower heating rates: for the $\beta = 10$ °C min⁻¹ analysis, the maximum releases are

detected at 102 °C for both species (see Table 3; Fig. 2). Actually, the E values obtained from the IC curve are slightly higher than those from the first TIC band, whose maximum evolution coherently occurs at lower temperatures. The same small shift is also observed in comparison of the behavior previously recorded for the pristine MgH₂ sample.

Activation energies of H₂O and CO₂ releases are compatible with a desorption process of chemically adsorbed molecules from the surface of the mixed SnO₂–MgH₂ matrix as described by the following reactions:



with a possible small contribution of the evolution of adsorbed water from the SnO₂ phase counterpart

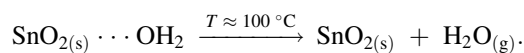


Table 5 Apparent activation energy values obtained, for SnO₂/MgH₂ = 0.2 sample, from TG–MS coupled measurements by using MS-data processed with Flynn–Wall–Ozawa (type B-0), Kissinger–Akahira–Sunose (type B-2), and Starink (type B-1.95 and 1.92) equations

| Data from | $T_{\text{isoconversion}}$ point from | Method | Linear equation from interpolated points ^a | R^{2b} | Act. energy/ kJ mol ⁻¹ | y value $y = E/RT$ |
|-------------|------------------------------------------------|--------|-------------------------------------------------------|----------|--------------------------------------|-----------------------|
| MS analysis | IC $m/z = 18$ curve 1st band T_{peak} | B-0 | $y = -4.3705x + 9.8443$ | 0.9986 | 35 ± 1 | 11 |
| | | B-2 | $y = -3.5988x - 4.068$ | 0.9978 | 30 ± 1 | 9 |
| | | B-1.95 | $y = -3.6181x - 3.7202$ | 0.9978 | 30 ± 1 | 9 |
| | | B-1.92 | $y = -3.6296x - 3.5115$ | 0.9979 | 30 ± 1 | 9 |
| | IC $m/z = 18$ curve 2nd band T_{peak} | B-0 | $y = -14.816x + 20.75$ | 0.9977 | 117 ± 2 | 21 |
| | | B-2 | $y = -13.483x + 5.7459$ | 0.9972 | 112 ± 3 | 20 |
| | | B-1.95 | $y = -13.516x + 6.121$ | 0.9972 | 112 ± 3 | 20 |
| | | B-1.92 | $y = -13.536x + 6.3461$ | 0.9972 | 112 ± 3 | 20 |
| | IC $m/z = 44$ curve 1st band T_{peak} | B-0 | $y = -4.6091x + 10.504$ | 0.9972 | 36 ± 1 | 11 |
| | | B-2 | $y = -3.8393x - 3.4033$ | 0.9956 | 32 ± 1 | 10 |
| | | B-1.95 | $y = -3.8586x - 3.0556$ | 0.9956 | 32 ± 1 | 10 |
| | | B-1.92 | $y = -3.8701x - 2.847$ | 0.9957 | 32 ± 1 | 10 |
| | IC $m/z = 44$ curve 2nd band T_{peak} | B-0 | $y = -11.191x + 19.462$ | 0.9988 | 88 ± 1 | 20 |
| | | B-2 | $y = -10.122x + 4.9003$ | 0.9985 | 84 ± 1 | 19 |
| | | B-1.95 | $y = -10.149x + 5.2643$ | 0.9985 | 84 ± 1 | 19 |
| | | B-1.92 | $y = -10.165x + 5.4827$ | 0.9985 | 84 ± 1 | 19 |
| | IC $m/z = 44$ curve 3rd band T_{peak} | B-0 | $y = -14.864x + 20.936$ | 0.9991 | 117 ± 2 | 21 |
| | | B-2 | $y = -13.538x + 5.9418$ | 0.9988 | 113 ± 2 | 20 |
| | | B-1.95 | $y = -13.571x + 6.3167$ | 0.9989 | 113 ± 2 | 20 |
| | | B-1.92 | $y = -13.591x + 6.5416$ | 0.9989 | 113 ± 2 | 20 |
| | IC $m/z = 2$ curve T_{peak} | B-0 | $y = -14.163x + 19.733$ | 0.9946 | 112 ± 4 | 20 |
| | | B-2 | $y = -12.827x + 4.7242$ | 0.9934 | 107 ± 4 | 19 |
| | | B-1.95 | $y = -12.86x + 5.0994$ | 0.9934 | 107 ± 4 | 19 |
| | | B-1.92 | $y = -12.88x + 5.3246$ | 0.9934 | 107 ± 4 | 19 |

^a From data reported in Table 3^b Correlation coefficient of the linear equation

A perfect coincidence of the activation energies (112–117 and 113–117 kJ mol⁻¹, respectively) was also found for the last release of H₂O and CO₂. In this doped sample these last H₂O and CO₂ evolutions are in correspondence with the hydrogen release event. These E values are slightly larger than those calculated from the second (and last) TIC-band (102–108 kJ mol⁻¹), but the differences are not highly significant with respect to the experimental errors. The top of their corresponding IC and TIC bands are practically detected at the same temperatures.

Activation energies of 84–88 kJ mol⁻¹ were calculated for the intermediate CO₂ release (centred at 253 °C for $\beta = 10$ °C min⁻¹). This process cannot be directly compared with the release of H₂O, as its evolution is broadened in a flat plateau that prevents a univocal determination of an isoconversion point. Nevertheless, these values are quite close to what previously found for water (88–94 kJ mol⁻¹) and carbon dioxide (88–94 kJ mol⁻¹) releases in the pristine MgH₂ sample, whose maxima occurred at 315 and 325 °C,

respectively ($\beta = 10$ °C min⁻¹). As discussed in the first part of this work [18], these last E values have been previously associated with the dehydration of magnesium hydroxide units and to the decarboxylation of those surface “magnesium carbonate-hydroxide species,” which constituted the impurity fraction of the pure MgH₂ matrix.

In the SnO₂-doped sample, analogous “metal carbonate-hydroxide species” could be considered present as amorphous layers on the surface of the metal oxide and of the MgH₂ crystallites, perhaps formed during the most delicate “air sensitive control process,” i.e., the milling. Again, these “metal-degraded units” can be responsible for the last relevant H₂O and CO₂ releases, which occur at a higher temperature and show an higher activation energy in comparison with the behavior previously studied of the pristine MgH₂ sample where the impurity counterpart accounts for a more aged and degraded MgH₂ reagent stock. Moreover, it must be reminded that differences in the “impurity component” of both the pristine MgH₂ and SnO₂-doped samples (as directly

obtained from XRD or as deduced from the minor H₂O and CO₂ releases in the MS data), must be compared considering that the XRD technique is particularly sensitive to the bulk crystalline structure and less sensitive to the presence of a thin amorphous layer. On the contrary, these superficial layers formed by the (chemical) degradation of the powdered samples are more easily detectable by the EGA in the TG–MS measurement, during the subsequent thermal treatment.

The most important thermal event of the SnO₂/MgH₂ = 0.2 specimen is the release of molecular hydrogen ($m/z = 2$ IC curve). From T_{peak} points, activation energies of 107–112 kJ mol⁻¹ were found. These values are all slightly higher than those found for the second TIC band. This result could be justified by considering that, differently from single ion currents, the TIC signal monitors the occurrence of the whole thermal process by averaging all its components: among these components we have also the incipient H₂ evolution due to the most reactive MgH₂ fraction formed in the milling process, as revealed by the initial flat plateau shown by the $m/z = 2$ IC trend.

Finally, the SnO₂/MgH₂ = 0.2 sample shows a net decrease of ca. 51–57 °C in the temperature of the main thermal decomposition event in comparison to the pristine MgH₂: the result is confirmed by TG, DTA and MS data. A reduction of the activation energy is coherently found, quantified as ca. 30 kJ mol⁻¹ if referred to the entire thermal process (as derived from TG, DTA, or TIC data) and as 28 kJ mol⁻¹, when it is specifically referred to hydrogen release (T_{peak} of the $m/z = 2$ IC). Concerning the first thermal event, attributed to the chemical desorption of H₂O and CO₂, the SnO₂/MgH₂ = 0, 2 sample presents an increase in the temperature of ca. 8.3 °C (detectable only by MS analysis by averaging the results from the T_{peak} points of TIC, $m/z = 18$ and 44 IC first bands) and a coherent increase in the associated activation energy of 11 kJ mol⁻¹. These facts could be attributed to the presence of the SnO₂ phase counterpart. The second initial event detected in the pristine MgH₂ sample, and associated to the release of H₂O from the dehydration of magnesium hydroxyl-species (second TIC and $m/z = 18$ bands), is negligible in the SnO₂-doped sample. On the contrary, the last H₂O and CO₂ release showed just by the doped sample can be again attributed to the metal carbonate-hydroxide species present on the surface of the degraded MgH₂, MgO, and SnO₂ crystallites: this release is detected at a higher temperature and involve a higher activation energy with respect to what was previously observed for the pristine MgH₂ sample.

Conclusions

The thermal behavior of undoped/unmilled MgH₂ and milled SnO₂-doped MgH₂ were analyzed and compared

using coupled TG–MS analyses. On the basis of the evolved gases, the thermal decomposition can be described throughout a sequence of chemical reactions occurring in the solid.

The reactions pattern provides relevant information concerning the chemical composition of the initial used reagents. In particular, we can assess the presence of a small degraded counterpart in the powder, probably constituted by amorphous complex metal carbonate–hydroxide–hydrate units present on the surface of the crystallites of the used reagents that was not detected by XRD.

The catalytic effects of SnO₂ doping and the beneficial effects of the high-energy mechanical milling used in the preparation of these samples were analyzed taking into account thermodynamic and kinetic parameters of the hydrogen thermal decomposition. Although a net decrease of the H₂ temperature release can be attributed to milling process, the addition of SnO₂ is beneficial to stabilize the β-MgH₂ and limiting the reduction in the quantity of released hydrogen. The SnO₂/MgH₂ = 0.2 specimen show a decrease of the hydrogen desorption of ca. 60–70 °C (up to 120 °C; depending on the kind of used signal: T_{onset} , T_{peak} of TG or MS data), associated to a decrease of the activation energy value of ca. 29–38 kcal mol⁻¹ (from MS data; a range of 25–79 kcal mol⁻¹ is obtained from TG data). The choice of the model-free iso-conversional methods to analyze the data (Kissinger–Akahira–Sunose; Flynn–Wall–Ozawa; Starink) has little influence on the result: the Flynn–Wall–Ozawa equation (type B-0) led to the best point interpolation ($R^2 \geq 0.994$) furnishing a higher value of the activation energy, with respect to the other laws (of ca. 4 kJ mol⁻¹).

Finally, the activation energies of water and carbon dioxide released from chemically adsorbed molecules were calculated and referred to processes where the correlated $y (= E/RT)$ values indicated an “improper use” of the various isoconversion methods ($y = 7$ –11). All the other observed thermal processes and reactions lead to activation energies values with a correct correlated y values ranging from 18 to 19, confirming the accuracy of the activation energy value determination.

References

1. Jain IP, Lal C, Jain A. Hydrogen storage in Mg: a most promising material. *Int J Hydrogen Energy*. 2010;35:5133–44.
2. Varin RA, Zbronic L, Polanski M, Bystrzycki J. A review of recent advances on the effects of microstructural refinement and nano-catalytic additives on the hydrogen storage properties of metal and complex hydrides. *Energies*. 2011;24(4):1–25.
3. Evard E, Gabis I, Yartys VA. Kinetics of hydrogen evolution from MgH₂: experimental studies, mechanism and modelling. *Int J Hydrogen Energy*. 2010;35:9060–9.

4. Varin RA, Czujko T, Wronski ZS. Particle size, grain size and γ - MgH_2 effects on the desorption properties of nanocrystalline commercial magnesium hydride processed by controlled mechanical milling. *Nanotechnology*. 2006;14(17):3856–65.
5. Hanada N, Ichikawa T, Fujii H. Catalytic effect of nanoparticle 3d-transition metals on hydrogen storage properties in magnesium hydride MgH_2 prepared by mechanical milling. *J Phys Chem B*. 2005;21(109):7188–94.
6. Hanada N, Ichikawa T, Orimo S-I, Fujii H. Correlation between hydrogen storage properties and structural characteristics in mechanically milled magnesium hydride MgH_2 . *J Alloys Compd*. 2004;366:269–73.
7. Bazzanella N, Checchetto R, Miotello A. Atoms and nanoparticles of transition metals as catalysts for hydrogen desorption from magnesium hydride. *J Nanomater*. 2011;2011:1–11.
8. Imamura H, Tanaka K, Kitazawa I, Sumi T, Sakata Y, Nakayama N, et al. Hydrogen storage properties of nanocrystalline MgH_2 and MgH_2/Sn nanocomposite synthesized by ball milling. *J Alloys Compd*. 2009;484:939–42.
9. Imamura H, Yoshihara K, Yoo M, Kitazawa I, Sakata Y. Dehydrogenation of Sn/MgH_2 nanocomposite formed by ball milling of MgH_2 with Sn. *Int J Hydrogen Energy*. 2007;32:4191–4.
10. Dufour J, Huot J. Rapid activation, enhanced hydrogen sorption kinetics and air resistance in laminated Mg-Pd_2 5 at.%. *J Alloys Compd*. 2007;439:L5–7.
11. Bassetti A, Bonetti E, Pasquini L, Montone A, Grbovic J, Vittori Antisari M. Hydrogen desorption from ball milled MgH_2 catalyzed with Fe. *Eur Phys J B*. 2005;11(43):19–27.
12. Zaluska A, Zaluski L, Ström-Olsen JO. Nanocrystalline magnesium for hydrogen storage. *J Alloys Compd*. 1999;288:217–25.
13. Patah A, Takasaki A, Szymd JS. Influence of multiple oxide ($\text{Cr}_2\text{O}_3/\text{Nb}_2\text{O}_5$) addition on the sorption kinetics of MgH_2 . *Int J Hydrogen Energy*. 2009;34:3032–7.
14. Kojima Y, Kawai Y, Haga T. Magnesium-based nano-composite materials for hydrogen storage. *J Alloys Compd*. 2006;424:294–8.
15. Barkhordarian G, Klassen T, Bormann R. Effect of Nb_2O_5 content on hydrogen reaction kinetics of Mg. *J Alloys Compd*. 2004;364:242–6.
16. Oelerich W, Klassen T, Bormann R. Metal oxides as catalysts for improved hydrogen sorption in nanocrystalline Mg-based materials. *J Alloys Compd*. 2001;315:237–42.
17. Malka IE, Czujko T, Bystrzycki J. Catalytic effect of halide additives ball milled with magnesium hydride. *Int J Hydrogen Energy*. 2010;35:1706–12.
18. Camprotrini R, Abdellatif M, Leoni M, Scardi P. Activation energy in the thermal decomposition of MgH_2 powders by coupled TG–MS measurements. Part I. Comparison among TG- and MS-data processing. *J Therm Anal Calorim*. 2014. doi:10.1007/s10973-013-3539-8 (in press).
19. Camprotrini R, Sicurelli A, Ischia M, Carturan G. Pyrolysis study of a hydride–sol–gel silica. Part I. Chemical aspects. *J Therm Anal Calorim*. 2007;19(89):633–41.
20. Camprotrini R, Sicurelli A, Ischia M, Carturan G. Pyrolysis study of a hydride–sol–gel silica. Part II. Kinetic aspects. *J Therm Anal Calorim*. 2007;22(90):179–84.
21. Camprotrini R, Ischia M, Palmisano L. Pyrolysis study of sol–gel derived TiO_2 powders: part I. TiO_2 -anatase prepared by reacting titanium(IV) isopropoxide with formic acid. *J Therm Anal Calorim*. 2003;71:13.
22. Camprotrini R, Ischia M, Palmisano L. Pyrolysis study of sol–gel derived TiO_2 powders: part II. TiO_2 -anatase prepared by reacting titanium(IV) isopropoxide with oxalic acid. *J Therm Anal Calorim*. 2003;71:1011–22.
23. Camprotrini R, Ischia M, Palmisano L. Pyrolysis study of sol–gel derived TiO_2 powders: part III. TiO_2 -anatase prepared by reacting titanium(IV) isopropoxide with acetic acid. *J Therm Anal Calorim*. 2004;75:13–24.
24. Camprotrini R, Ischia M, Palmisano L. Pyrolysis study of sol–gel derived TiO_2 powders: part IV. TiO_2 -anatase prepared by hydrolysing titanium(IV) isopropoxide without chelating agents. *J Therm Anal Calorim*. 2004;75:25–34.
25. Young RA. “Ray.” *The Rietveld method*. IUCr Monograph on Crystallography. New York: Oxford University Press; 1993.
26. Abdellatif M, Camprotrini R, Leoni M, Scardi P. Effects of SnO_2 on hydrogen desorption of MgH_2 . *Int J Hydrogen Energy*. 2013;38:4664–9.
27. Kissinger HE. Variation of peak temperature with heating rate in differential thermal analysis. *J Res Natl Bur Stand*. 1956;57:217.
28. Flynn JH, Wall LA. A quick, direct method for the determination of activation energy from thermogravimetric data. *J Polym Sci B*. 1966;4:323–8.
29. Ozawa T. Estimation of activation energy by isoconversion methods. *Thermochim Acta*. 1992;203:159–65.
30. Starink MJ. A new method for the derivation of activation energies from experiments performed at constant heating rate. *Thermochim Acta*. 1996;288:97–104.
31. Murray P, White J. Kinetics of the thermal dehydration of clays: part IV. Interpretation of the differential thermal analysis of clay minerals. *Trans Br Ceram Soc*. 1955;54:204–37.
32. Starink MJ. The determination of activation energy from linear heating rate experiments: a comparison of the accuracy of isoconversion methods. *Thermochim Acta*. 2003;404:163–76.
33. Starink MJ. Activation energy determination for linear heating experiments: deviations due to neglecting the low temperature end of the temperature integral. *J Mater Sci*. 2007;11(42):483–9.